



Relativistic Quantum Scars

Liang Huang,¹ Ying-Cheng Lai,^{1,2} David K. Ferry,^{1,2,3} Stephen M. Goodnick,^{1,2,3} and Richard Akis^{1,3}

¹*Department of Electrical Engineering, Arizona State University, Tempe, Arizona 85287, USA*

²*Department of Physics, Arizona State University, Tempe, Arizona 85287, USA*

³*Center for Solid State Electronics Research, Arizona State University, Tempe, Arizona 85287, USA*

(Received 27 February 2009; published 27 July 2009)

The concentrations of wave functions about classical periodic orbits, or quantum scars, are a fundamental phenomenon in physics. An open question is whether scarring can occur in relativistic quantum systems. To address this question, we investigate confinements made of graphene whose classical dynamics are chaotic and find unequivocal evidence of relativistic quantum scars. The scarred states can lead to strong conductance fluctuations in the corresponding open quantum dots via the mechanism of resonant transmission.

DOI: 10.1103/PhysRevLett.103.054101

PACS numbers: 05.45.Mt, 03.65.Pm, 73.63.-b

A remarkable phenomenon in quantum systems whose dynamics in the classical limit are chaotic is scarring. In particular, in the semiclassical regime a wave function can be regarded locally as a superposition of many plane waves. Because of classical chaos, the directions of these plane waves are uniformly distributed. Intuitively, one may expect the wave functions to have uniform concentration in the position space. Signatures of nonuniform distribution of the wave function were, however, discovered by McDonald and Kaufman in their study of the Helmholtz equation in the classically chaotic stadium billiard [1]. Numerical investigations of the system in the semiclassical regime by Heller [2] revealed the striking “scarring” phenomenon that the wave functions tend to concentrate on paths corresponding to unstable periodic orbits in the classical limit. Theoretical explanations of the scarring effect were provided by Bogomolny [3] and Berry [4] based on the semiclassical Green’s function. Since then the phenomenon of quantum scars has become an active area of research in nonlinear physics [5,6].

Existing works on scarring are concerned exclusively with nonrelativistic quantum mechanical systems described by the Schrödinger equation, where the dependence of the particle energy on momentum is quadratic. A question is whether scarring can occur in relativistic quantum systems described by the Dirac equation, where the energy-momentum relation is linear. This question, besides being fundamental to basic physics, has also become important in device applications. In particular, graphene, a single, one-atom-thick sheet of carbon atoms arranged in a honeycomb lattice, has recently been realized in experiments [7]. Because of its peculiar hexagonal lattice structure, the band structure exhibits a linear dependence of the energy on the wave vector about the Dirac points, signifying relativistic motion. Indeed, electrons in graphene behave like massless Dirac fermions, and have Fermi velocity $v_F \approx 10^6$ m/s [8]. Devices made of graphene are potentially capable of operating at much higher speed than those based on the conventional silicon elec-

tronics. A common class of systems in device research is quantum dots, where some geometric structure of graphene is connected with a number of graphene nanoribbons (leads). Possible scarring states can have significant effect on electronic transport through the dot [9]. In particular, since scars generally can lead to pointer states [10] in open quantum dots, conductance fluctuations can arise. Furthermore, pointer states associated with more pronounced scars in the corresponding closed system indicate longer trapping time of the electrons in the quantum dot, which can lead to narrower conductance resonant peaks (or dips). Therefore, from the properties of scars in the closed system one can infer the extent of conductance fluctuations in the corresponding open system.

In this Letter, we present results on quantum scarring in closed graphene confinements exhibiting chaotic dynamics in the classical limit. A fairly representative class of such confinements is stadiums. Using the tight-binding approach, we calculate the wave functions both in the low-energy regime where the particle motions obey the Dirac equation and in the high-energy regime where the trigonal warping distortion becomes dominant [11,12]. Our calculations and analysis reveal unequivocal signatures of pronounced concentrations of eigenwave functions about classical periodic orbits.

The Hamiltonian of a closed graphene system is given by $\hat{H} = \sum (-t)|i\rangle\langle j|$, where the summation is over all pairs of nearest neighbors, and $t \approx 2.8$ eV is the nearest-neighbor hopping energy [13]. The on-site energy has been neglected as we assume it is the same for all carbon atoms in the confinement. The eigenenergies and the associated wave functions can then be calculated. To be concrete, we first consider a stadium-shaped graphene system, where we have removed boundary atoms with only one neighbor to avoid possible artificial scattering effects. Three typical patterns of electron concentration are shown in Figs. 1(a)–1(c) for three distinct energy levels. Since the system is relatively large, the $E - \mathbf{k}$ relation for an infinite graphene flake can be used to gain insight. The allowed

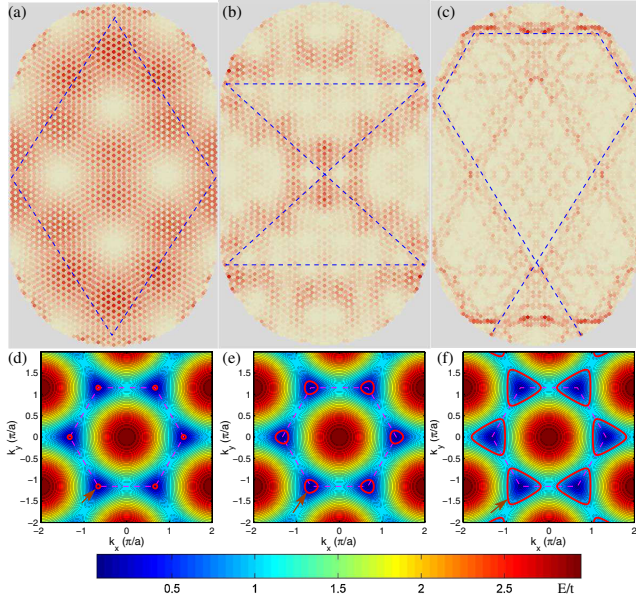


FIG. 1 (color online). Typical quantum scars [red (darker region) indicates higher electron concentration] for a stadium-shaped graphene confinement with zigzag horizontal boundaries and contour plots of energy in the wave vector plane (the band structure). The energies for the patterns in (a–c) are $E/t = 0.13252, 0.4024,$ and $0.91188,$ respectively. The stadium consists of $N = 11814$ carbon atoms. Panels (d–f) show the $E - \mathbf{k}$ configuration for an infinite graphene flake for the same lattice orientation and energy values as those for (a–c), respectively. The allowed wave vectors are on the constant energy curves (as indicated by the arrows). The lattice constant is $a = 2.46 \text{ \AA}$. Dashed line segments in (a–c) are for eye guidance, and in (d–f) they indicate the first Brillouin zone.

wave vectors for the specific energies of the patterns are shown in Figs. 1(d)–1(f). Note that for an infinite system, the allowed wave vectors constitute continuous curves in the contour plots of energy versus the wave vector. For a finite confinement, the allowed wave vectors are discrete. In the following, we discuss mechanisms for scars in low-, intermediate-, and high-energy regimes.

Low-energy regime ($E/t \ll 1$).—In this regime, the possible wave vectors are restrained to the vicinity of the Dirac points, as indicated by the small solid circles in Fig. 1(d). In addition, the number of allowed wave vectors is small so that any quantum superposition consists of only a few allowed plane waves. Along the directions perpendicular to those from the origin to the Dirac points, the wavelength $\lambda \sim 2\pi/k_{\perp}$ is large, where k_{\perp} is the perpendicular component of the allowed wave vectors. For two plane waves of close wave vectors, say, $\mathbf{k}_1 = \mathbf{K} + \mathbf{k}_{\perp}/2$ and $\mathbf{k}_2 = \mathbf{K} - \mathbf{k}_{\perp}/2$, where $\mathbf{k}_{\perp} \perp \mathbf{K}$, the composed wave is given by $e^{i\mathbf{k}_1 \cdot \mathbf{x} + \phi_1} + e^{i\mathbf{k}_2 \cdot \mathbf{x} + \phi_2} = 2 \cos[\mathbf{k}_{\perp} \cdot \mathbf{x}/2 + (\phi_1 - \phi_2)/2] e^{i\mathbf{K} \cdot \mathbf{x} + (\phi_1 + \phi_2)/2}$, representing a propagating wave along the direction \mathbf{K} modulated by a standing wave in the perpendicular direction. The antinode is given by $\cos[\mathbf{k}_{\perp} \cdot \mathbf{x}/2 + (\phi_1 - \phi_2)/2] = 0$ so that the distance between the nearby antinodes is $2\pi/|\mathbf{k}_{\perp}|$. Since $|\mathbf{K}|$ is gen-

erally large (of the order of π/a), the wavelength along the \mathbf{K} direction is small (extending a few lattice sites). Similar analysis holds for other allowed wave vectors. For certain energy values, the superposition of the allowed plane waves forms standing waves, as shown in Fig. 1(a). As suggested by our analysis, the antinodes of the standing waves (light region in the figure) have three directions only, which are parallel to the directions from the origin to the Dirac points.

Intermediate-energy regime ($E/t < 1$).—In this regime, there are many allowed wave vectors, and they form nearly continuous contour lines (constant energy curves) in the wave vector space [Fig. 1(e)]. As a result, the plane waves for each line segment of the allowed wave vectors generate a wave packet with group velocity determined by the gradient of the energy with respect to wave vector. The width of the wave packet is of the order of $\pi/|\Delta\mathbf{k}|$, where $|\Delta\mathbf{k}|$ is the width of the allowed wave vectors perpendicular to the direction of the group velocity. The contour lines are approximately circles, indicating that the particle motion can take on any directions. As the linear relation between energy and wave vector holds in this energy range, the scars formed in this case are thus relativistic quantum scars. Since the group velocity can be in any direction, the orientations of the scarred patterns can be in any direction as well. The widths of the scars are typically large since $\Delta\mathbf{k}$ is still small about the Dirac points.

For slightly larger energy values, the constant energy curves acquire a nontrivial distortion, the so-called trigonal warping [11]. Although there is some tendency for the group velocity to focus on the three directions, as suggested by Fig. 1(e), the velocity can be in any direction depending on the boundary conditions. Figure 1(b) provides such an example. Note that the diagonal line patterns are not along the directions from the origin to the Dirac points.

High-energy regime ($E/t \sim 1$).—In this regime, the trigonal warping becomes more dominant, and the linear relation between energy and the amplitude of wave vector in the vicinity of the Dirac points, originally held in the low- and intermediate-energy regimes, is now violated, as shown in Fig. 1(f). The group velocity is proportional to the gradient $\nabla_{\mathbf{k}} E$, which is locally perpendicular to the constant energy curve. From Fig. 1(f), we see that the group velocity focuses on only three directions, i.e., those from the origin to the Dirac points. Since the zigzag boundaries are along the horizontal direction, the directions are 0 (or π), $\pi/3$ ($4\pi/3$), and $2\pi/3$ ($5\pi/3$) in phase angles [14].

To understand the “sharpness” of the scars in this regime, we consider the following simplified situation. Assume the wave vector can take on values in a line segment $[\mathbf{k}_1, \mathbf{k}_2]$, and let $\mathbf{k}_m = (\mathbf{k}_1 + \mathbf{k}_2)/2$ and $\Delta\mathbf{k} = (\mathbf{k}_2 - \mathbf{k}_1)$. If N allowed wave vectors are distributed uniformly on the line segment, the superposition of the corresponding plane waves is $\sum_{\mathbf{k}} e^{i\mathbf{k} \cdot \mathbf{x}} \times |\Delta\mathbf{k}|/N \approx \int_{\mathbf{k}_1}^{\mathbf{k}_2} e^{i\mathbf{k} \cdot \mathbf{x}} d\mathbf{k} = e^{i\mathbf{k}_m \cdot \mathbf{x}} |\Delta\mathbf{k}| \sin(\Delta\mathbf{k} \cdot \mathbf{x}/2) / [\Delta\mathbf{k} \cdot \mathbf{x}/2]$, which is in fact a

propagating wave of wave vector \mathbf{k}_m modulated by the $\sin u/u$ term, where $u = \Delta\mathbf{k} \cdot \mathbf{x}/2$. The modulation factor causes the wave to focus on a narrow linear region of width $\lambda = 4\pi/|\Delta\mathbf{k}|$, which is perpendicular to $\Delta\mathbf{k}$. Since $|\Delta\mathbf{k}|$ for each constant energy line segment is of the order of π/a , λ can be as small as a few unit cells, generating highly concentrated scars. Depending on the symmetry of the confinement, the scars can have different shapes. However, the line segments forming these scars can only assume three directions. Figure 1(c) shows two symmetrical closed orbits. One can see that the line patterns are indeed quite sharp.

Effects of lattice orientation.—The $E - \mathbf{k}$ structure of graphene has a hexagonal symmetry for the locations of the Dirac points in the wave vector space [Fig. 1(d)], even though the two nearby Dirac points are inequivalent. Figures 2 and 3 show some typical scars for the same stadium confinement with different lattice orientations, e.g., zigzag and armchair in the horizontal direction. In the high-energy regime, the orientations of the scars are determined by the trigonal warping that has only three directions pointing from the origin to the Dirac points. As the $E - \mathbf{k}$ structures in Figs. 2 and 3 have a $\pi/2$ difference, the patterns of the scars in the two figures also exhibit a $\pi/2$ difference. This explains the horizontal line patterns in Fig. 2 and the vertical line patterns in Fig. 3 for high-energy cases. The final scar formation depends also on the confinement shape so that its symmetry will manifest in the scars [15]. Furthermore, only when a closed orbit has segments in the three allowed directions, as determined by the lattice orientation, can a scar be formed.

We now briefly address the consequence of scars on electronic transmission in open graphene quantum dots.

We consider an open stadium-shaped quantum dot, as shown in Fig. 4(a) and calculate the transmission [16]. For conventional semiconductor quantum dots, scars can lead to strong transmission fluctuations in small energy scales [17]. Such fluctuations have also been observed in our graphene quantum dots, as shown in Figs. 4(b) and 4(c). The difference between the two cases is that for Fig. 4(c), two carbon atoms [indicated by the arrow in Fig. 4(a)] are removed so as to break the mirror symmetry. We see that the fluctuations tend to be less sharp in Fig. 4(c). This is consistent with our finding (data not shown) that in the underlying closed graphene system, symmetry breaking tends to smear out scars that would otherwise be sharp.

As the energy or the wave number varies, scars appear and disappear repeatedly. From the semiclassical theory [18], two successive scars associated with the same classical periodic orbit occur when the action integral satisfies the condition $\Delta S = h$, where h is the Planck constant. Since $S = \oint \mathbf{p}d\mathbf{q}$ and \mathbf{p} has the same direction as $d\mathbf{q}$, for a given periodic orbit of length L , we have $S = |\mathbf{p}|L = \hbar|\mathbf{k}|L$. For a conventional semiconductor confinement, the electron energy is $E = \hbar^2k^2/(2m_e)$. In this case, \sqrt{E} is equally spaced for scars associated with the same periodic orbit [19]. For graphene confinement, $E = \hbar v_F k$ for low energy, where $v_F = \sqrt{3}ta/(2\hbar)$ is the Fermi velocity, and $k = |\Delta\mathbf{k}|$ is the magnitude of the wave vector from the Dirac points; therefore, it is E which is equally spaced for recurring scars. In particular, the energy interval for scars focusing on a given periodic orbit is determined by $h = \hbar\Delta|\mathbf{k}|L = (\Delta E/v_F)L$, or $\Delta E = \hbar v_F/L$. We have identified series of recurring patterns for the one shown in Fig. 1(b) and the one in Fig. 3(a). For Fig. 1(b), the energy

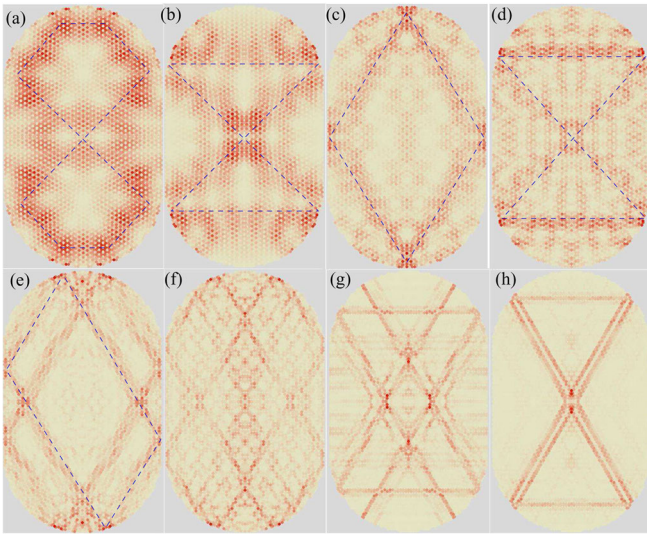


FIG. 2 (color online). Typical scars in the stadium-shaped graphene confinement as in Fig. 1. The energy values for (a–h) are $E/t = 0.25347, 0.36358, 0.57665, 0.60699, 0.81956, 0.91061, 0.97722, \text{ and } 0.99198$, respectively. The dashed lines represent classical periodic orbits.

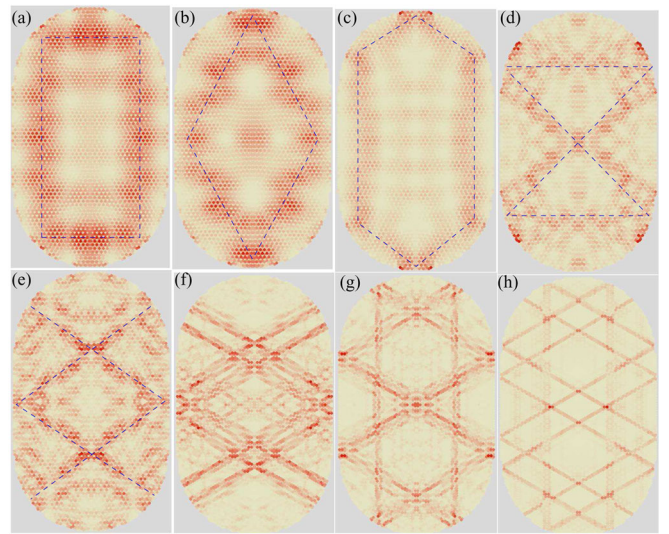


FIG. 3 (color online). Scars in stadium-shaped graphene confinement with armchair horizontal boundaries. The number of atoms is $N = 13694$. The corresponding energy values are $E/t = 0.20031, 0.2599, 0.3106, 0.54954, 0.59238, 0.9168, 0.95216, \text{ and } 0.99801$ for (a–h), respectively.

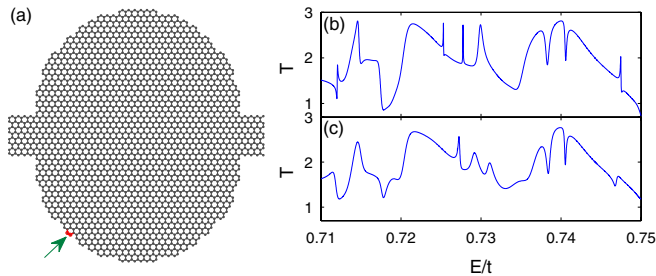


FIG. 4 (color online). (a) An open stadium-shaped graphene quantum dot with semi-infinite leads on both sides. The shape has a mirror symmetry. (b) Transmission T versus energy E/t . (c) Transmission T for the dot after removing the two carbon atoms as indicated by the arrow in (a) so that the mirror symmetry is broken.

interval between consecutive scars is $0.0195t$, the length of the orbit is $275a = 67.65$ nm, leading to $\Delta E = 0.0198t$. For scars similar to Fig. 3(a), the energy interval is $0.0203t$, while the length of the orbit is $263a = 64.70$ nm, yielding $\Delta E = 0.0207t$, which agrees well with the numeric observations. This corroborates the linear relation between energy and wave vector, which is a unique feature of scarring in graphene systems and fundamentally different from that in conventional quantum systems.

The existence of relativistic quantum scars can also be argued heuristically from the Dirac equation: $-i\hbar v_F \sigma \cdot \nabla \Psi = E\Psi$, where σ is Pauli's matrices and $\Psi = [\Psi_A, \Psi_B]^T$ is a two component spinor describing the two types of nonequivalent atoms in graphene [13]. Each component, by itself, satisfies the Helmholtz equation. Thus the scars in relativistic quantum systems have the same origin as those arising in contexts such as water surface waves, vibrating blocks, ultrasonic fields, microwave billiards, and quantum dot billiards [6]. Nevertheless, relativistic quantum scars are distinct from the conventional quantum scars in terms of features such as the recurrence with respect to energy variation.

In summary, using graphene as a paradigm, we have discovered relativistic quantum scars for both closed and open systems, and investigated the mechanism for the formation of various scarring patterns in different energy regimes. As in conventional semiconductor quantum dots, scars can lead to strong transmission (conductance) fluctuations.

This work was supported by AFOSR under Grant No. FA9550-09-1-0260 and by ONR under Grant No. N0014-08-1-0627.

- [1] S. W. McDonald and A. N. Kaufman, Phys. Rev. Lett. **42**, 1189 (1979); Phys. Rev. A **37**, 3067 (1988).
 [2] E. J. Heller, Phys. Rev. Lett. **53**, 1515 (1984).
 [3] E. B. Bogomolny, Physica (Amsterdam) **31D**, 169 (1988).
 [4] M. V. Berry, Proc. R. Soc. A **423**, 219 (1989).

- [5] M. C. Gutzwiller, *Chaos in Classical and Quantum Mechanics* (Springer, New York, 1990).
 [6] H. J. Stöckmann, *Quantum Chaos: An Introduction* (Cambridge University Press, Cambridge, England, 1999).
 [7] K. S. Novoselov, A. K. Geim, S. V. Morozov, D. Jiang, Y. Zhang, S. V. Dubonos, I. V. Grigorieva, and A. A. Firsov, Science **306**, 666 (2004).
 [8] K. S. Novoselov, A. K. Geim, S. V. Morozov, D. Jiang, M. I. Katsnelson, I. V. Grigorieva, S. V. Dubonos, and A. A. Firsov, Nature (London) **438**, 197 (2005).
 [9] R. A. Jalabert, H. U. Baranger, and A. D. Stone, Phys. Rev. Lett. **65**, 2442 (1990); H. U. Baranger, R. A. Jalabert, and A. D. Stone, Phys. Rev. Lett. **70**, 3876 (1993); C. M. Marcus, A. J. Rimberg, R. M. Westervelt, P. F. Hopkins, and A. C. Gossard, Phys. Rev. Lett. **69**, 506 (1992); T. M. Fromhold, L. Eaves, F. W. Sheard, M. L. Leadbeater, T. J. Foster, and P. C. Main, Phys. Rev. Lett. **72**, 2608 (1994); T. M. Fromhold, P. B. Wilkinson, F. W. Sheard, L. Eaves, J. Miao, and G. Edwards, Phys. Rev. Lett. **75**, 1142 (1995).
 [10] W. H. Zurek, Rev. Mod. Phys. **75**, 715 (2003).
 [11] R. Saito, G. Dresselhaus, and M. S. Dresselhaus, Phys. Rev. B **61**, 2981 (2000); J. L. Garcia-Pomar, A. Cortijo, and M. Nieto-Vesperinas, Phys. Rev. Lett. **100**, 236801 (2008).
 [12] The warped energy bands lead to anisotropy of the effective mass, a possible origin of chaotic electron motion. See, for example, T. M. Fromhold *et al.*, Nature (London) **428**, 726 (2004).
 [13] A. H. Castro Neto, F. Guinea, N. M. R. Peres, K. S. Novoselov, and A. K. Geim, Rev. Mod. Phys. **81**, 109 (2009).
 [14] In the presence of a magnetic field, the band structure of graphene changes, and the scars vary accordingly. We have examined scars of stadium-shaped graphene confinement in a perpendicular magnetic field and found that, for weak field, the corresponding classical orbits of the scars are almost unchanged, but when the field is strong and the energies become quantized, the scars smear out and some new orbits (both straight and curved) appear. When spin effects are included, the scarring orbits could be more complicated.
 [15] Because of the discrete nature of the lattice, in the high-energy regime where the quantum wavelength is on the order of the lattice constant, the roughness at the edge needs to be taken into account to determine the effective shape of the billiard.
 [16] S. Datta, *Electronic Transport in Mesoscopic Systems* (Cambridge University Press, Cambridge, England, 1995).
 [17] D. K. Ferry, R. Akis, and J. P. Bird, Phys. Rev. Lett. **93**, 026803 (2004); R. Brunner, R. Meisels, F. Kuchar, R. Akis, D. K. Ferry, and J. P. Bird, Phys. Rev. Lett. **98**, 204101 (2007); R. Brunner, R. Akis, D. K. Ferry, F. Kuchar, and R. Meisels, Phys. Rev. Lett. **101**, 024102 (2008).
 [18] M. C. Gutzwiller, J. Math. Phys. (N.Y.) **12**, 343 (1971).
 [19] D. A. Wisniacki, F. Borondo, E. Vergini, and R. M. Benito, Phys. Rev. E **62**, R7583 (2000); D. A. Wisniacki, E. Vergini, R. M. Benito, and F. Borondo, Phys. Rev. Lett. **94**, 054101 (2005); **97**, 094101 (2006).